

Dynacortin Is a Novel Actin Bundling Protein That Localizes to Dynamic Actin Structures*

Received for publication, December 19, 2001
Published, JBC Papers in Press, January 8, 2002, DOI 10.1074/jbc.M112144200

Douglas N. Robinson‡, Stephani S. Ocon, Ronald S. Rock, and James A. Spudich§

From the Department of Biochemistry, Stanford University School of Medicine, Stanford, California 94305-5307

Dynacortin is a novel protein that was discovered in a genetic suppressor screen of a *Dictyostelium discoideum* cytokinesis-deficient mutant cell line devoid of the cleavage furrow actin bundling protein, cortexillin I. While dynacortin is highly enriched in the cortex, particularly in cell-surface protrusions, it is excluded from the cleavage furrow cortex during cytokinesis. Here, we describe the biochemical characterization of this new protein. Purified dynacortin is an 80-kDa dimer with a large 5.7-nm Stokes radius. Dynacortin cross-links actin filaments into parallel arrays with a mole ratio of one dimer to 1.3 actin monomers and a 3.1 μM K_d . Using total internal reflection fluorescence microscopy, GFP-dynacortin and the actin bundling protein coronin-GFP are seen to concentrate in highly dynamic cortical structures with assembly and disassembly half-lives of about 15 s. These results indicate that cells have evolved different actin-filament cross-linking proteins with complementary cellular distributions that collaborate to orchestrate complex cell shape changes.

Cellular morphogenesis results from regional forces that work against the global material properties of the cell (reviewed in Ref. 1). Changes in the cortical shape of a cell depend primarily on the actin filament network. Localized forces are either expansive as the result of new actin filament polymerization or contractile typically as a result of the activity of actin-based motor proteins of the myosin superfamily. The cell's material properties include the stiffness and surface tension, which are determined, in part, by the cross-linking of the actin cortical cytoskeleton. Actin-associated proteins determine the stability and the degree of cross-linking of the filament network and may help to identify the locations where expansive and contractile force generation may occur.

Cytokinesis is an elegant cellular process because both contractile force generation and new actin filament polymerization act in concert to produce the desired dynamic shape changes. A role for global and spatial activities has been well observed in *Dictyostelium discoideum* cytokinesis. Factors that are globally distributed and factors recruited to the cleavage furrow are

both required for cytokinesis (reviewed in Ref. 2). Genetically, an interaction between global and regional proteins has been demonstrated and from this at least two interacting genetic modules have been proposed to control cytokinesis (3). The first module includes the actin-binding proteins cortexillin I and myosin-II (4, 5). Myosin-II is a force generating protein that probably produces the majority of the force required for cell cleavage. Cortexillin I was originally identified biochemically as an actin filament-binding protein and has been demonstrated to collaborate with myosin-II to define a spatially restricted midzone of contractility (6). The second module is a global pathway that is controlled by the RacE small GTPase and includes dynacortin and the actin bundling protein coronin (3, 7, 8). Three of these proteins, RacE, myosin-II, and cortexillin I, have been shown to contribute to the bending modulus and/or surface tension (also in-plane elasticity) of the cell (9–11).

Dynacortin, originally discovered in a suppressor screen of a *cortexillin I* mutant cell line, is a novel protein of low complexity (100 hydroxyamino acids out of 354 total amino acids) (3). The protein is distributed globally in the cell cortex and becomes enriched in cell surface protrusions. During cell division, it maintains its global cortical association, becomes enriched at the ruffling poles of the cell and appears to be diminished in the cleavage furrow. This is in stark contrast to the high enrichment of cortexillin I and myosin-II in the cleavage furrow cortex during this time (12, 13). Furthermore, the distribution of dynacortin and the actin cross-linking protein coronin along the lateral cortex (regions between protrusions) depends on the RacE small GTPase. Dynacortin is a soluble phosphoprotein that is found in a complex with a large Stokes radius. Using a library complementation system for *D. discoideum*, a truncated cDNA of dynacortin, which encodes the carboxyl 181 amino acids of the protein, was isolated by its ability to suppress the loss of cortexillin I. In contrast, the full-length version of dynacortin did not suppress the *cortexillin I* mutants. Expression of the truncated protein caused a downshift in the apparent Stokes radius of the endogenous dynacortin complex, suggesting that the native dynacortin complex is multimeric. Together, these observations suggest that the suppressing version of dynacortin may be interrupting normal dynacortin function. Identification of dynacortin's biochemical activity is essential to understand the function of the protein complex and to begin to understand how perturbing this global activity can compensate for the loss of cortexillin I.

In this paper, we describe the purification of the native dynacortin complex from *D. discoideum* and demonstrate that it is homomeric. Since the purified protein from *D. discoideum* was limiting in amount, we expressed and purified a recombinant form from *Escherichia coli*. The recombinant protein has an identical Stokes radius to the native *D. discoideum* complex and directly binds and bundles actin filaments into complex

* This work was supported by a Burroughs Wellcome Career Development Award (to D. N. R.), a Helen Hay Whitney postdoctoral fellowship (to R. S. R.), and National Institutes of Health Grant GM40509 (to J. A. S.). The costs of publication of this article were defrayed in part by the payment of page charges. This article must therefore be hereby marked "advertisement" in accordance with 18 U.S.C. Section 1734 solely to indicate this fact.

‡ To whom correspondence may be addressed. Current address: Dept. of Cell Biology, Johns Hopkins University School of Medicine, 725 N. Wolfe St., Baltimore, MD 21205. Tel.: 410-502-2850; E-mail: Douglas.Robinson@jhu.edu.

§ To whom correspondence may be addressed. E-mail: jspudich@cmgm.stanford.edu.

arrays. The dissociation constant and the native cellular concentrations of this protein complex support a model whereby this soluble complex can directly bind and bundle actin filaments *in vivo*. Finally, using total internal reflection fluorescence microscopy, we demonstrate that dynacortin associates with dynamic cortical structures. All of our data indicate that cells have evolved different actin cross-linkers that localize in distinct regions of the cell but that collaborate to promote complex cell shape changes.

MATERIALS AND METHODS

Cell Culture and DNA Manipulations

D. discoideum cells were grown in standard DdHL-5 media (14). For large scale preparations, 24 liters of cells were grown 2 liters at a time in 6-liter flasks while shaking at 200 rpm. Cells were grown to late log phase (as they just approached $\sim 1 \times 10^7$ cells/ml) before harvesting.

For *E. coli*, BL21-CodonPlus(DE3)-RIL cells (Stratagene) were grown in standard LB with ampicillin and chloramphenicol for plasmid selection. Protein expression was induced when the cells reached an optical density at 600 nm of 0.6. Then, isopropyl-1-thio- β -D-galactopyranoside was added to 1 mM and cells were allowed to grow an additional 4 h before harvesting.

For the *E. coli* expression plasmid, His-dynacortin pET14b, the dynacortin cDNA was moved from a precursor plasmid of pLD1A15SN:GFP¹-dynacortin (3) into pET28b using *Sall* and *NotI* flanking restriction sites. The His tag, protease site, and T7 epitope tag along with the dynacortin cDNA were moved from pET28b using flanking *NcoI* and *NotI* sites into pET14b. This allows ampicillin to be used for plasmid selection rather than kanamycin, which is required for pET28b. The GFP-dynacortin and coronin-GFP constructs were described previously (3) and the GFP-RacE was generated in the same pLD1A15SN vector using a GFP tagging cassette as described for the dynacortin and coronin GFP fusion vectors (3).

Native *D. discoideum* Dynacortin Purification

For a purification experiment, typically 500 g of log-phase *D. discoideum* cells were used as starting material. Cells were harvested by centrifugation. The cell pellet was washed one time in 10 mM Tris, pH 7.4. Pellets were resuspended in cell lysis buffer (20 mM NaCl, 20 mM Na₂VO₄, 150 mM Hepes pH 7.1, 1 mM EGTA, 1 mM EDTA), and a mixture of protease inhibitors including the following: 0.1 mM phenylmethylsulfonyl fluoride, 150 μ M 1-chloro-3-tosamido-7-amino-2-heptanone, 80 μ g/ml L-1-tosylamido-2-phenylethyl chloromethyl ketone, 1 μ g/ml benzamidine, 100 μ g/ml *N* α -p-tosyl-L-arginine-methyl ester, and 5 μ g/ml leupeptin. Cells were lysed by freeze/thaw using liquid nitrogen. After lysis, extracts were centrifuged at 17,000 \times g for 30 min at 4 °C. The supernatants were decanted and polyethyleneimine was added to a final concentration of 0.23%. Lysates were stirred gently for 5 min at 22 °C. This cationic polymer allows the precipitation of negatively charged molecules such as nucleic acids and monomeric actin. Lysates were centrifuged again at 17,000 \times g for 15 min at 4 °C, which resulted in complete clearing of the supernatant. The supernatant was collected and solid ammonium sulfate was added gradually to 45% saturation. After stirring gently for 15 min, the sample was centrifuged for 15 min at 17,000 \times g at 4 °C. The 0–45% ammonium sulfate fraction was recovered for subsequent chromatographic steps. Nearly 100% of the dynacortin was recovered during these initial precipitation steps as judged by Western analysis of supernatant and pellet fractions (Fig. 1A). The first significant loss occurred during the dialysis of the large ammonium sulfate pellet. However, the apparent yield was higher, approaching 300%, after the polyethyleneimine precipitation probably as a result of epitope exposure as nucleic acids and lipids were removed from the preparation.

All chromatography steps were performed using either a Amersham Biosciences, Inc. FPLC system or a Waters MPLC system. All resins and prepacked columns were purchased from Amersham Biosciences, Inc. unless otherwise indicated. The *D. discoideum* ammonium sulfate pellet was resuspended in Buffer A (20 mM NaCl, 25 mM Hepes pH 7.1, 1 mM EDTA, 1 mM EGTA with the mixture of protease inhibitors). The solution was dialyzed overnight against the same buffer. After dialysis the solution of protein was collected, centrifuged at 48,000 \times g for 20 min to remove insoluble materials, and the protein concentration was

determined using the Bio-Rad Protein Assay. The protein concentration was adjusted to less than 10 mg/ml for ion exchange. Typically, about 4 g of protein were recovered after the ammonium sulfate separation from 500 g of cells, which meant the volume was adjusted to about 400 ml. No more than 2 g of protein were applied to a 200-ml SP-Sepharose Fast Flow column at a time to prevent saturation of the resin. The Buffer A used was adjusted to pH 7.1. During initial development of the purification procedure, pH 6.5 and 8 were also tested. Only pH 7.1 allowed nearly 100% of the dynacortin to bind to the SP-Sepharose resin. After application, the protein was eluted in a linear gradient from 0% Buffer B to 65% Buffer B over 20 column volumes. Buffer B was the following: 1 M NaCl, 25 mM Hepes pH 7.1, 1 mM EDTA, and 1 mM EGTA. Because it took two runs to separate the entire sample, the dynacortin peaks, which centered around 7–8 mS/cm conductivity were recovered and combined, concentrated by 60% ammonium sulfate precipitation, and resuspended in 12 ml of Buffer A. This material was applied to a Sephacryl S300 26/60 size exclusion column equilibrated in gel filtration buffer (50 mM NaCl, 25 mM Hepes pH 7.1, 1 mM EDTA, 1 mM EGTA). The protein eluted from this column at approximately $K_{av} = 0.25$. The first half of the peak was collected; the second half was discarded because of a large fraction of contaminants. The protein was diluted 2-fold and applied to a Mono Q HR 10/10 column equilibrated in Buffer A. The flow-through was collected, concentrated on a Mono S HR 5/5 column using a step gradient and separated on a Mono P HR 5/5 column equilibrated at pH 7 using the chromatofocusing buffer system 96 and 74. The protein was eluted with a pH 7–6 gradient using the manufacturer's suggested buffer combination for this pH range (Amersham Biosciences Inc.). Two peaks of protein were eluted, a minor peak with an apparent pI of ~ 7.2 and a second major peak with an apparent pI of 6.8. The second peak (apparent pI = 6.8) was applied to a Sephadex S200 10/30 size exclusion column. The protein eluted with a $K_{av} = 0.18$ on this column, comparable to the native unpurified and partially purified dynacortin complex.

Recombinant Dynacortin Purification

Since His-dynacortin was not well overexpressed in *E. coli*, presumably because of codon usage bias, a more elaborate purification protocol was required than may be typical for recombinantly expressed proteins. Cells were recovered by centrifugation and pellets were resuspended in the same buffer as *D. discoideum* cells except with only 10 mM Hepes pH 7.1 and without the 20 mM Na₂VO₄. *E. coli* cells were lysed with three passes through a French press at 1200 psi. Lysates were prepared exactly as the *D. discoideum* extracts with the polyethyleneimine precipitation and ammonium sulfate precipitation at 45% saturation. As with the native *D. discoideum* protein, only minimal dynacortin loss during these initial steps was detected by Western analysis. The ammonium sulfate pellets derived from *E. coli* lysates were resuspended in 12 ml of 10 mM Hepes pH 7.1 and were applied to the S300 26/60 size exclusion column equilibrated in 200 mM NaCl, 10 mM Hepes pH 7.1. The protein eluted at the same place as native dynacortin with an approximate $K_{av} = 0.25$. The appropriate fractions were pooled and applied to an 8-ml Ni²⁺/NTA (Qiagen) superflow resin column pre-equilibrated with "no salt" Buffer A (10 mM Hepes pH 7.1 only). After binding, the column was washed in no salt Buffer A and the protein was eluted with a gradient from 0% no salt Buffer B to 100% no salt Buffer B (10 mM Hepes, 500 mM imidazole, pH 8.0) in 8 column volumes. The peak of His-dynacortin was pooled and applied to a Mono S HR 5/5 column equilibrated in no salt Buffer A. The protein was eluted with a 22-column volume segmented salt gradient from 0% Buffer B to 100% Buffer B (1 M NaCl, 25 mM Hepes pH 7.1, 1 mM EDTA, and 1 mM EGTA). Recovered protein was pooled, diluted in no salt Buffer A and reappplied to the Mono S but was eluted with a 50% Buffer B step elution. This concentrated the protein for dialysis. For actin binding studies, the dynacortin was dialyzed overnight in 2 mM NaCl, 10 mM Hepes pH 7.1, 1 mM Na₂S₂O₃. For analytical ultracentrifugation, it was dialyzed into the same buffer except with 400 mM NaCl. Typically, around 0.3 mg of purified dynacortin were recovered per liter of cells and 10 liters of cells were used per purification.

Analysis by Analytical Ultracentrifugation

To determine the stoichiometry of the His-tagged dynacortin, the protein was subjected to equilibrium sedimentation analysis using a Beckman Optima XL-A analytical ultracentrifuge (Beckman Instruments). The monomer molecular mass of the purified protein was calculated to be 42,286 Da from the primary sequence. This was verified by matrix-assisted laser desorption ionization-time of flight mass spectroscopy using a Perseptive Voyager-DE RP Biospectrometry instrument

¹ The abbreviations used are: GFP, green fluorescent protein; MES, 4-morpholineethanesulfonic acid; $M_{w,app}$, apparent molecular weight.

(Stanford PAN Facility) where the monomer mass was determined to be 42,332 Da. The partial specific volume was calculated to be 0.715 ml/g. The solvent density was calculated for different salt concentrations by summing the incremental density contributions of the constituents. All calculations including temperature corrections were made by Laue's methods (15). The solvents contained 128, 264, or 400 mM NaCl. The buffer contained 10 mM Hepes pH 7.1. Initial protein concentrations ranged from 7.5 to 30 μ M protein. Protein concentration was monitored by absorption at 280 nm. Initial concentration readings were taken at 3,000 rpm. The samples were centrifuged at 9,000, 11,000, 12,000, and 15,000 rpm for at least 26 h, then scans were taken every 2–4 h until the sample reached equilibrium. Absorption curves were integrated after equilibrium and compared with the integrated absorption of the initial scan at 3,000 rpm. The fractional amount of protein in the cell after reaching equilibrium compared with the initial sample was 1.0 ± 0.02 ($n = 12$; mean \pm S.E.), verifying that the measured molecular weight is accurately reflecting the population of protein and that there is no significant loss due to precipitation during the centrifugation. The $M_{w,app}$ was determined by fitting multiple data files to a single ideal species. Data were also fit to a model of an associating system of a monomer-dimer equilibrium. All fits were performed using the Microcal Origin software (Beckman Instruments).

Analysis of Actin Binding Properties

In Vitro Cosedimentation—Chicken skeletal G-actin was prepared from chicken breast using standard purification methods (16). The actin was allowed to polymerize at high concentrations for 15 min at 22 °C by the addition of $\times 10$ polymerization buffer (500 mM KCl, 10 mM $MgCl_2$, 10 mM EGTA, 2 mM ATP, 10 mM dithiothreitol, 100 mM imidazole, pH 7 (17), to a final concentration of $1 \times$ polymerization buffer). Both actin and His-dynacortin were centrifuged to remove any aggregates before the assays were performed. Actin and His-dynacortin were mixed to appropriate concentrations and His-dynacortin dialysis buffer was added to normalize the volume of His-dynacortin buffer. The reactions contained a final concentration of $1 \times$ polymerization buffer. Samples were incubated for 1 h at 22 °C and sedimented at $100,000 \times g$ (total actin binding) in a TL100 ultracentrifuge for 20 min or at $10,000 \times g$ (actin bundling) in a microcentrifuge for 20 min. Supernatant and pellet fractions were collected, resuspended to a final concentration of $1 \times$ Laemmli's sample buffer and equivalent amounts were loaded on 15% SDS-PAGE gels. Gels were stained in Coomassie Blue stain and destained in 10% acetic acid. Proteins were quantitated using an Alphamager 2000 scanning densitometer (Alpha Innotech Corp.). The linear ranges for dynacortin and actin concentrations were determined so only appropriate amounts at each concentration were loaded on the gel for accurate quantitation.

Electron Microscopy—Various concentrations of His-dynacortin and 2 μ M F-actin were mixed in $1 \times$ polymerization buffer and incubated for ~ 1 h. Carbon-coated copper grids were incubated with the protein mixture for 2 min. The grids were washed two times in filtered $1 \times$ polymerization buffer or water and then grids were incubated in 2% uranyl acetate for times ranging from 2 to 4 min. Grids were allowed to air dry and were imaged using a Philips CM-12 electron microscope.

Fluorescence Microscopy—To examine the formation of actin bundles by light microscopy, actin filaments were stabilized with tetramethyl rhodamine-labeled phalloidin (Molecular Probes). Dynacortin was mixed with labeled actin filaments and viewed. Alternatively, flow cells were prepared so that different proteins could be added sequentially. Typically, actin filaments (1 μ M) were sheared by 10 passages through a 26-gauge needle and added to the flow cell. Then dynacortin (3–5 μ M) was added to one edge of the cell while on the sample stage. This allowed a gradient of dynacortin to form. Actin filament arrays and rings were observed but were biased to different regions of the gradient. The buffer used in flow cell experiments was 25 mM KCl, 25 mM imidazole, pH 7.4, 1 mM EGTA, 4 mM $MgCl_2$, 10 mM dithiothreitol.

Cellular Concentration of Dynacortin

To determine the cellular concentration of dynacortin, whole *D. discoideum* cell lysates were prepared in cell lysis buffer from DH1 and Ax2 strains. Concentrations were determined using a Bio-Rad Protein Assay. Purified His-dynacortin was used as a standard and its concentration was determined using the calculated extinction coefficient, $19,060 \text{ M}^{-1} \text{ cm}^{-1}$. Dilution series of each protein sample were separated by SDS-PAGE and transferred to nitrocellulose. The dynacortin protein was detected using rabbit anti-dynacortin polyclonal sera (diluted 1 to 40,000) (3) and goat anti-rabbit antibodies conjugated to horseradish peroxidase (Bio-Rad) (diluted 1 to 10,000). Immune complexes were

detected using enzyme-coupled chemiluminescence (Amersham Biosciences Inc.). Dynacortin bands were quantitated by densitometry and densities were plotted *versus* the amount of input protein. The resulting lines were fit to a linear equation to identify the linear range. The densities from the five points from Ax2 and DH1 cells that fell in the linear range of the purified recombinant standard line were used to calculate the amount of dynacortin in the sample. After multiplying this amount by 2.9 to correct for epitope exposure observed during the purification of native dynacortin from *D. discoideum* (Fig. 1A, from the 290% yield during the first few steps of the purification), the protein represents 0.07% of the total cellular protein. To determine the concentration of dynacortin in the cell, the average diameter of *D. discoideum* cells removed from plates was estimated to be 8 μ m using a Coulter Counter (Beckman Coulter). This permitted the rough calculation of the cell's volume, assuming that the cell is a simple sphere. The total cellular protein concentration was measured to be 60 μ g/ 10^6 cells, which is in reasonable agreement with the published concentration of 50 μ g/ 10^6 cells (18).

Total Internal Reflection Microscopy

To monitor the dynamics of the GFP fusion proteins *in vivo*, cells were imaged in MES starvation buffer (25 mM KCl, 20 mM MES, pH 6.8, 2 mM $MgSO_4$, and 0.2 mM $CaCl_2$) using a through the objective total internal reflection microscope. Excitation light was provided by a 488-nm argon ion laser (Melles Griot) and a $\times 100$ (NA 1.65) objective (Olympus) was used for imaging. Cells were imaged in homemade anodized aluminum imaging chambers through 1.78 refractive index coverglasses. Emission light was collected using a Princeton Instruments PentaMAX intensified CCD and images were collected and processed using Winview (Roper Scientific). One-s frames were collected every second for 200–400 frames. The movies were analyzed using NIH Image. Regions of interest were monitored by tabulating the modal intensity within a 100 pixel² (0.367 μ m²) region *versus* time. Time frames of interest were fit to a single exponential equation to determine the rates of intensity change using KaleidaGraph (Synergy Software).

RESULTS

Purification of Native *D. discoideum* and Recombinant Dynacortin—In our previous study, we determined that native *D. discoideum* dynacortin separated on a size exclusion column with a large apparent Stokes radius of about 5.7 nm (3). To determine whether this complex is homomeric or heteromeric, we have purified it from *D. discoideum*. We developed a purification scheme that comprised polyethyleneimine and ammonium sulfate precipitations followed by a series of ion exchange, size exclusion, and chromatofocusing columns (Fig. 1A, see "Materials and Methods"). During the early phases of developing a purification protocol, it was difficult to purify the protein to homogeneity. This was partly due to the fact that dynacortin always eluted in somewhat broad peaks typically spanning a 30 mM change of salt concentration, probably due to multiple phosphorylation states of the protein. The difficulty also derived from the fact that dynacortin and the actin-related protein complex 2/3 (Arp2/3; reviewed in Refs. 19 and 20) showed considerable overlap in their fractionation properties on cationic and anionic exchange resins and by size exclusion. Both complexes also showed considerable co-fractionation on a Mono P column by chromatofocusing using a pH range of 7 to 5. However, by adjusting the ionic strength of the fractions pooled from the size exclusion column to 25 mM salt (conductivity about 3 mS/cm), all of the Arp2/3 complex bound to a Mono Q HR 10/10 column and much of the dynacortin also bound. However, a small amount of dynacortin (less than 25%) did not bind to this resin under these conditions. This protein was concentrated on a Mono S column and further fractionated on a Mono P column by chromatofocusing using an elution gradient of pH 7 to 6 (Fig. 1B). This protocol provided nearly complete purification as judged by SDS-PAGE gels (a 4300-fold enrichment; see below) although the yields were too small to accurately quantitate the amount of recovery at this point. Sufficient quantities of protein were recovered, however, for size exclusion characterization with detection by Western im-

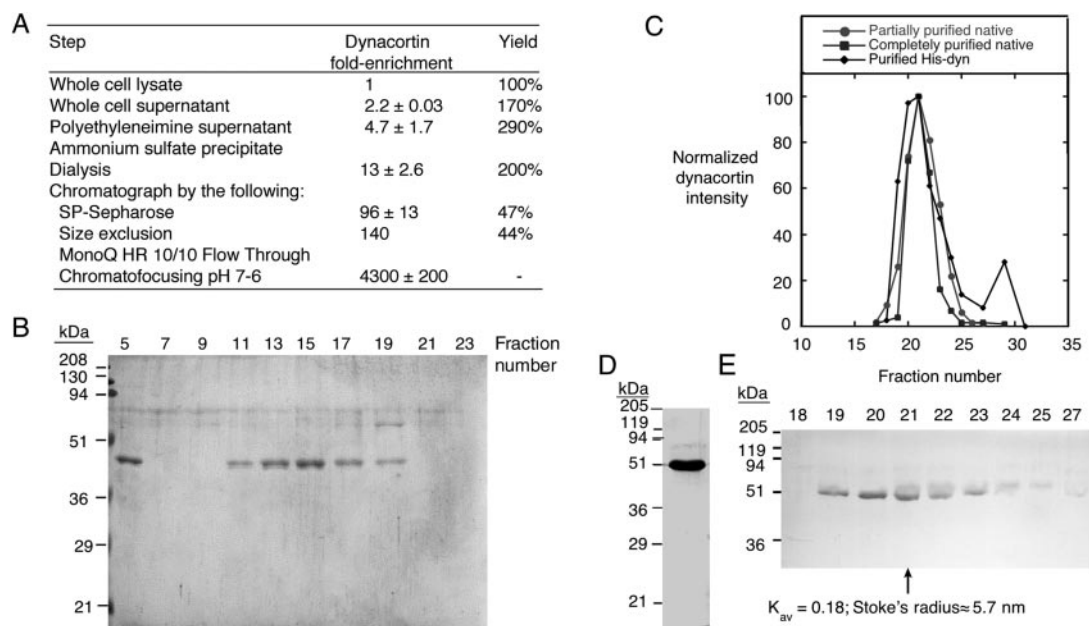


FIG. 1. Purification of native *D. discoideum* and recombinant dynacortin proteins. *A*, a table showing the steps of purification of native dynacortin with the degree of purification (relative enrichment of dynacortin relative to total protein) and the yields indicated. *B*, a Coomassie-stained gel of fractions collected from a chromatofocusing separation of purified native dynacortin. *C*, a plot of normalized dynacortin density of partially purified and completely purified native dynacortin and recombinantly expressed His-dynacortin proteins separated by high resolution size exclusion chromatography using a Sephadex S200 10/30 column. *D*, an example of purified *E. coli* expressed recombinant His-dynacortin separated on a Coomassie-stained SDS-PAGE gel. *E*, a Coomassie-stained SDS-PAGE gel of fractions from the size exclusion experiment in *C*, using His-dynacortin. The fraction numbers of the gel correspond to the fraction numbers of the density trace in *C*. The recombinant His-dynacortin, like the native dynacortin, elutes with a K_{av} of ~ 0.18 and an apparent Stokes radius of about 5.7 nm.

munoblot analysis, and the purified protein had an identical size to the unpurified (not shown) and partially purified native *D. discoideum* dynacortin (Fig. 1C). With the assurance that the native complex is homomeric (not heteromeric) and because the yields were so small, we purified recombinantly expressed His-tagged dynacortin from *E. coli* (Fig. 1D). This recombinant protein had an identical elution profile from the same size exclusion column as the native *D. discoideum* complex (Fig. 1, C and E). We used the recombinant His-dynacortin for further biochemical studies.

Because the protein has such a large Stokes radius even though the monomer molecular weight (M_r) is only 37,800 for the native dynacortin protein and 42,300 for the His-tagged recombinant protein, we performed sedimentation equilibrium analysis of the recombinant protein to determine the stoichiometry of the complex. The apparent molecular weight ($M_{W,app}$) was 67,000 when the protein species was modeled as a single ideal species. This $M_{W,app}$ was independent of ionic strength, solvent density, and relative centrifugal force. The ratio of $M_{W,app}$ to M_r is 1.59 (67.0/42.3). A few possibilities exist: the protein could be an associating system of a monomer-dimer, the protein could be nonideal, or both. Nonideality can occur if the protein is particularly asymmetric in shape or can result from charge effects. A decrease in $M_{W,app}$ with increasing protein concentration is a strong indicator of nonideality and this trend was observed for dynacortin (not shown). We also used multiple data sets from a variety of speeds and modeled the system as an associating monomer-dimer. The best fits were obtained if the second virial coefficient was allowed to vary (settling on 6.5×10^{-6}) and the association constant was at least 10^7 M^{-1} . An example of this fit to one of the data sets along with the residuals is shown (Fig. 2). Thus, at micromolar concentrations and because of its monodispersity by size exclusion chromatography, the sedimentation equilibrium data strongly indicate dynacortin is a dimer. Furthermore, given its dimer molecular weight and large Stokes radius, dynacortin is most likely highly asymmetric in shape.

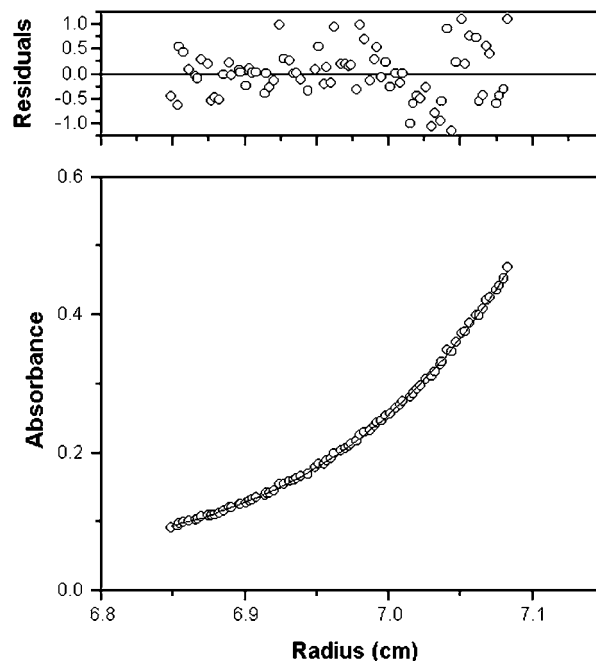


FIG. 2. Analytical ultracentrifugation analysis of the stoichiometry of the His-dynacortin complex. Presented is an example of a fit (curved line) and the residuals from one data set (circles) to a model of a monomer-dimer associating system in which the molecular weight of the monomer is 42,286, the complex is a dimer ($n = 2$), the second virial coefficient is 6.51223×10^{-6} , and $K_a = 10^7 \text{ M}^{-1}$. The fit parameters were acquired by fitting the model simultaneously to 10 data sets ($X^2 = 5.77125$, $df = 781$, $p > 0.20$).

Characterization of Dynacortin's Actin Binding Properties— Since dynacortin localizes to actin-rich cortical domains of the cell (3), we tested whether the protein could bind actin filaments *in vitro* using cosedimentation assays. The protein co-

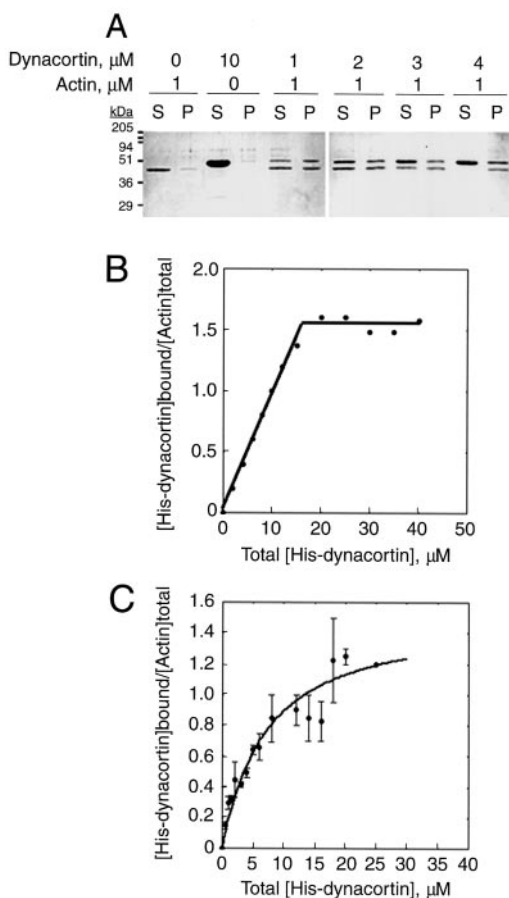


FIG. 3. Dynacortin binds and bundles actin filaments *in vitro*. *A*, dynacortin and actin filaments co-sediment at $10,000 \times g$, whereas neither protein alone sediments into a pellet under these conditions. The concentration of dynacortin is based upon the monomer concentration. This experiment was performed under low salt (5 mM KCl) conditions. *B*, using sedimentation force of $100,000 \times g$, dynacortin titrated with $10 \mu\text{M}$ filamentous actin saturating at $15 \mu\text{M}$ bound dynacortin. One representative titration curve is presented. This saturation of 1.5 mol of monomeric dynacortin (0.75 mol of dimers) to 1 mol of monomer actin leads to the binding model $1D_2 + 1A_{1.3} \leftrightarrow 1D_2A_{1.3}$. It should be noted that fractional actin (1.3 mol of actin) is possible since the actin is polymeric. The saturation ratio was independent of the salt conditions. *C*, an example of a binding curve. The average K_d was calculated to be $3.1 \pm 0.24 \mu\text{M}$. The fit is the calculated binding curve with a K_d of $3.1 \mu\text{M}$ and agrees well with the data ($X^2 = 0.29827$, $df = 14$, $p > 0.20$). The salt conditions for the binding experiments were $1 \times$ polymerization buffer (50 mM KCl).

sedimented with actin in both high-speed (total binding) and low-speed (bundling) assays, whereas in the absence of actin filaments, it remained in the supernatant fraction under both conditions. An example gel showing dynacortin and actin sedimenting at low speed is shown (Fig. 3A). To determine the stoichiometry and affinity of dynacortin's actin binding activity, we used the high-speed sedimentation conditions where all of the polymerized actin sediments, allowing total binding to be measured. Under conditions of medium salt ($1 \times$ polymerization buffer which contains 50 mM KCl), $10 \mu\text{M}$ filamentous actin was titrated with dynacortin (Fig. 3B). 100% of the dynacortin bound to the actin up to nearly $15 \mu\text{M}$ dynacortin, calculated from the monomer molecular weight. The binding saturated at 1.5 mol of dynacortin (0.75 mol of dynacortin dimers) to 1 mol of actin. This results in a binding model where 1 mol of dynacortin dimer saturates 1.3 mol of actin. By lowering the actin concentration to 1–2 μM under the same salt conditions, the dynacortin-actin interaction entered the "binding" regime where the fraction bound varied around 50% and allowed the

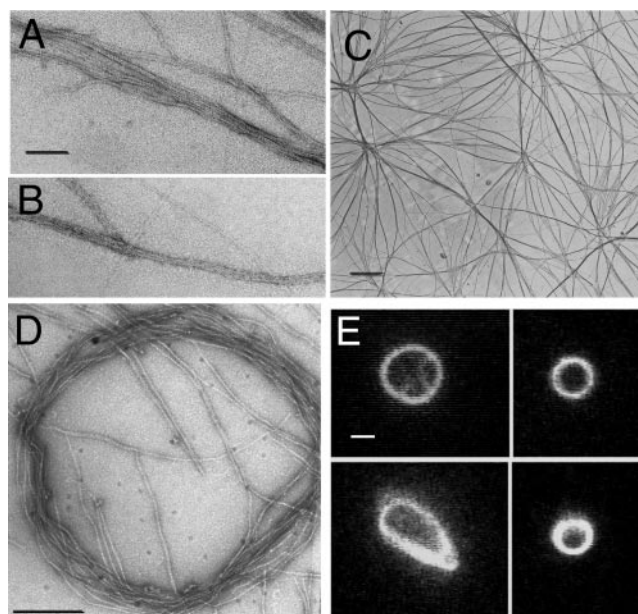


FIG. 4. Dynacortin bundles actin filaments into parallel arrays. *A*, a dynacortin bundle was constructed then diluted to allow some of the dynacortin to dissociate. Constituent actin filaments are easily observed in the frayed bundles. *Scale bar* in *A* is 50 nm and applies to *A* and *B*. *B*, a saturated actin filament bundle with dynacortin ($10 \mu\text{M}$ dynacortin, $5 \mu\text{M}$ actin). *C*, elaborate arrays of dynacortin-actin filament bundles are often observed with bundles routinely reaching 100 nm in diameter and in some cases much larger. *Scale bar* is 2 μm . *D*, dynacortin frequently bundles actin filaments into circular arrays or rings. *Scale bar* is 0.5 μm . *E*, dynacortin-actin rings can be visualized by fluorescence microscopy when the actin filaments are labeled with fluorophore-labeled phalloidin. Four examples are shown. *Scale bar* is 1 μm .

dissociation constant to be accurately measured (Fig. 3C). By using the binding model in Fig. 3B, the mean K_d was calculated to be $3.1 \pm 0.24 \mu\text{M}$ ($n = 25$; mean \pm S.E.). The measured K_d was between 2 and 4 μM using dynacortin from three different protein preparations. By lowering the salt concentration to 5 mM KCl, dynacortin and actin interactions were in titration range at submicromolar concentrations, indicating that the interaction is salt dependent. Given the high affinity, it was not possible to accurately measure the K_d of total binding interactions in 5 mM KCl using the high-speed sedimentation assay. However, the same saturation ratio of 1 dynacortin dimer per 1.3 actins was observed under these salt conditions. We were able to measure the apparent affinity (K_d) for bundling under these salt conditions, which was $390 \pm 50 \text{ nM}$ ($n = 7$).

The finding that dynacortin co-sediments with actin filaments at low speeds ($10,000 \times g$) suggests that dynacortin may cross-link actin into complex arrays. We examined the proteins by electron microscopy using uranyl acetate negative staining and fluorescence microscopy using fluorescent phalloidin-stabilized actin filaments. In the actin-alone controls, individual actin filaments were observed. When the actin was mixed with dynacortin, the actin was organized into large parallel arrays (Fig. 4, *A* and *B*). These arrays could be quite extensive having diameters typically in the range of 100–1000 nm in diameter. The bundles could also interlock, forming complex arrays (Fig. 4C). Surprisingly, dynacortin also organized the actin filaments into rings (Fig. 4, *D* and *E*). These rings were very uniform in shape and typically ranged from 2 to 5 μm in diameter. By electron microscopy, it is apparent that these rings consist of circular arrays of actin filament bundles (Fig. 4D).

This recombinant dynacortin was used as a standard to determine the cellular concentration of native *D. discoideum*

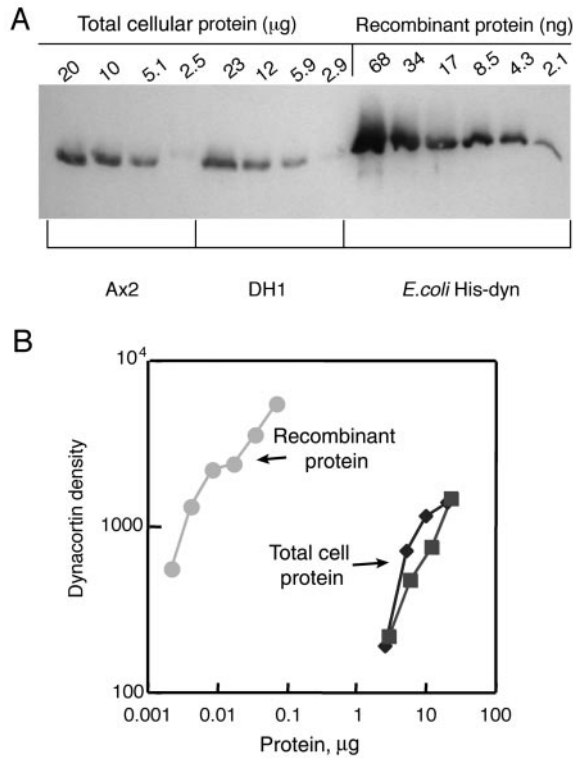


FIG. 5. The cellular concentration of monomeric dynacortin is ~4 μM. *A*, quantitative Western analysis reveals the amount of dynacortin in cells. A dilution series of total cell lysates from Ax2 and DH1 cells are compared with a dilution series of purified His-dynacortin. *B*, the densities of each band were quantitated and plotted against the protein amount. The data from the recombinant protein was fit to a linear equation. Points from the whole cell lysates that fell within the range of this line were substituted into the linear fit equation to calculate the amount of dynacortin in the lysate. By dividing the dynacortin equivalent in nanograms by the number of micrograms of total cell protein, the fraction of total cell protein was determined. The average for both strains was 4300 ± 200 . Then, by making a $2.9 \times$ correction for epitope exposure from Fig. 1, the cellular concentration of dynacortin monomer was determined to be about 4 μM. The data from the DH1 cells is plotted as *black diamonds*, data from Ax2 cells are plotted as *dark squares*, and data from purified recombinant His-dynacortin are plotted as *light gray circles*.

dynacortin (Fig. 5). The cellular concentrations of dynacortin are in the range of 4 μM (2 μM dimer).

Analysis of Dynacortin Dynamics in Cells—In our previous work (3), we demonstrated that dynacortin co-localizes with actin and the actin bundling protein coronin in the cell cortex, particularly at cell surface protrusions such as pseudopodia and actin crowns. Example epifluorescence images of GFP-dynacortin, coronin-GFP, and GFP-RacE small GTPase are shown (Fig. 6, A–C). Cells expressing GFP-dynacortin have dynacortin-rich actin rings (Fig. 6A, *arrow*), structures that may be the *in vivo* correlates of the dynacortin-actin rings constructed *in vitro* (Fig. 4, D and E). To get an idea of the dynamic nature of the dynacortin-rich and coronin-rich structures, we have complemented our previous work by using total internal reflection fluorescence microscopy. This technique takes advantage of an evanescent wave created by the reflected light at the boundary between the glass and solution and allows illumination of an exponentially decaying field on the order of 100–200 nm from the surface of the coverslip. This allows the cell surface to be continuously illuminated for video rate imaging while generating an image that is completely in focus. By epifluorescence imaging, cells cannot tolerate continuous illumination for long periods of time. Using total internal reflection fluorescence imaging, we

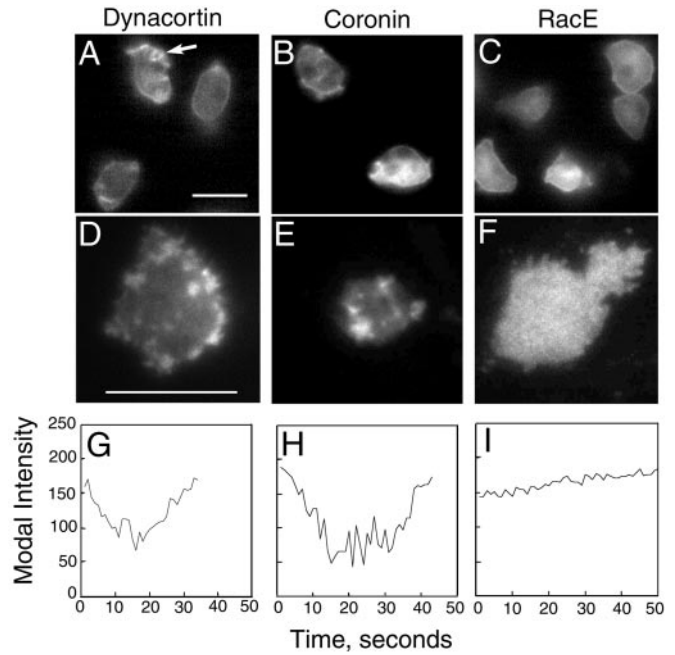


FIG. 6. Epifluorescence and total internal reflection microscopy reveals that dynacortin associates with dynamic actin structures. *A*, *D*, and *G*, GFP-dynacortin. *B*, *E*, and *H*, coronin-GFP. *C*, *F*, and *I*, GFP-RacE. *A*–*C*, epifluorescence images showing cortical localization of all three proteins. Dynacortin and coronin also are enriched in surface protrusions. A dynacortin-rich ring is identified by the *arrow* in *A*. *D*–*F*, total internal reflection microscopy shows dynacortin and coronin enrichment in surface structures whereas RacE is uniformly distributed. *G*–*I*, example modal intensity traces of 100 pixel² regions of each protein. It should be noted that NIH Image treats black regions or absence of signal as the maximal color intensity and white regions or maximal signal as the minimal color intensity. Thus, a decrease in modal intensity reflects an increase in GFP accumulation and vice versa. *Scale bar* in *A* applies to *A*–*C* and *scale bar* in *D* applies to *D*–*F*. *Scale bars*, 10 μm.

monitored the distribution of GFP-dynacortin, coronin-GFP, and GFP-RacE for up to 15 min with continuous illumination without apparent deleterious effects on the cells (Fig. 6, D–I). Both dynacortin and coronin were highly dynamic localizing to structures that formed and dissipated. We also electroporated cells with rhodamine-labeled rabbit skeletal globular actin. Qualitatively, the rhodamine actin formed similar structures; however, because the cells were less healthy from the electroporation, we did not examine them further (not shown). RacE, on the other hand, was uniformly distributed along the surface of the cell. Since RacE has a carboxyl-terminal prenylation motif (8), it is likely tethered directly to the plasma membrane and so is reflecting the position of the membrane. We quantitated the dynamics of the GFP-dynacortin, coronin-GFP, and GFP-RacE by monitoring the modal intensity of the fluorescence within a 100-pixel² region over time. Example traces are shown (Fig. 6, G–I). The regions of the traces that were either growing or decaying were fit to a single exponential equation and rates, correlation coefficients, and the half-lives were calculated (Table I). Dynacortin and coronin showed very similar kinetics of accumulation and dissipation whereas RacE did not show any increase, only a very slow decrease, which may be due to photobleaching. Together, these data indicate that dynacortin is a novel actin bundling protein that concentrates with highly dynamic actin-rich cell surface structures.

DISCUSSION

Dynacortin is a novel protein discovered in *D. discoideum* by library complementation and multicopy suppression of a cyto-

TABLE I

Quantitation of the dynamics GFP-dynacortin, coronin-GFP, and GFP-RacE at the ventral cell surface

It should be noted that NIH Image treats black regions or absence of signal as the maximal color intensity and white regions or maximal signal as the minimal color intensity. Thus, a decrease in modal intensity reflects an increase in GFP accumulation and *vice versa*. Therefore, the signs of growth are negative and the signs of decay are positive. k is the rate constant in s^{-1} ; R is the correlation coefficient from the fits of the data to a single exponential, and $t_{1/2}$ is the calculated half-time. All differences between GFP-dynacortin and GFP-coronin are not significant: $p > 0.10$. GFP-RacE is significantly different from the other two: $p < 0.00005$ (one tailed t -test).

Protein	$k_{(\text{growth})} \pm \text{S.E.}$	$R \pm \text{S.E.} (n)$	$t_{1/2}$	$k_{(\text{decay})} \pm \text{S.E.}$	$R \pm \text{S.E.} (n)$	$t_{1/2}$
GFP-dynacortin	-0.050 ± 0.007	$0.88 \pm 0.019 (28)$	14 s	0.035 ± 0.004	$0.89 \pm 0.013 (28)$	20 s
Coronin-GFP	-0.056 ± 0.010	$0.87 \pm 0.020 (17)$	12 s	0.055 ± 0.015	$0.84 \pm 0.031 (13)$	13 s
GFP-RacE				0.0018 ± 0.00056	$0.61 \pm 0.060 (18)$	390 s

kinesis-deficient strain of cells devoid of cortexillin I (3). Cortexillin I is an actin filament-bundling protein that is highly enriched in the cleavage furrow cortex during cytokinesis (5, 13). A construct of dynacortin was isolated in a genetic selection experiment designed to select for suppressors of *cortexillin I*. The *cortexillin I* suppressing version of dynacortin included only the carboxyl 181 amino acids (about half) of the protein. This construct also caused a downshift in the apparent size of the endogenous dynacortin. Since the full-length dynacortin construct failed to complement the *cortexillin I* mutant and in fact caused a dominant cytokinesis defect, it is likely that the suppressor molecule was functioning as a dominant-negative mutation. Furthermore, dynacortin is distributed around the cell cortex during cytokinesis, appears excluded or reduced in the cleavage furrow cortex, and becomes enriched in the polar ruffles.

A genetic model for cytokinesis in which the global shape control pathway (dynacortin, coronin, and RacE) is antagonized by the equatorial contractile pathway (cortexillin I and myosin-II) has been proposed to integrate these observations (3) (Fig. 7). Here, we demonstrate that dynacortin is a novel actin filament-bundling protein. Since cytokinesis is a mechanical process, it is likely that actin bundling proteins contribute to the material properties of the cell, creating spatially restricted regions (stiffness persistence) that allow the cortex to be remodeled in specific ways (1). Indeed, using atomic force microscopy, regional stiffness differences have been observed in mammalian cell culture cells undergoing cytokinesis (21). The myosin-II, cortexillins, and RacE proteins are known to be required for membrane bending stiffness and surface tension (also in-plane elasticity) (9–11). Since the normal distribution of dynacortin depends, in part, on the RacE small GTPase, it is plausible that dynacortin contributes to a global cell stiffness. Dynacortin's actin filament bundling activity is consistent with a role in cell stiffness.

These observations suggest that cells have evolved different actin filament bundling activities that reside in different locations in the cell to orchestrate complex cell shape changes (Fig. 7). Using distinct actin bundling activities may allow cells to more easily regulate the actin cross-linking activities in specific ways and may possibly allow different types of structures to be assembled. Dynacortin is a phosphoprotein and phosphorylation may modulate the localization and/or actin bundling activity of the protein. Given the cellular concentrations of actin filaments ($70 \mu\text{M}$) (22) and dynacortin dimers ($2 \mu\text{M}$) and the measured K_d of the His-dynacortin-actin interaction *in vitro* ($3 \mu\text{M}$), 90% of the dynacortin could be bound to actin in the cell. Yet, dynacortin is soluble in crude extracts (3). Since dynacortin binding to actin filaments is affected by ionic strength it is very plausible that phosphorylation could affect the K_d for actin binding by affecting the on or off rates or both. Indeed, understanding dynacortin's phosphorylation may be crucial to understanding the *in vivo* regulation of dynacortin's actin filament bundling activity.

Dynacortin depends on the RacE small GTPase for localiza-

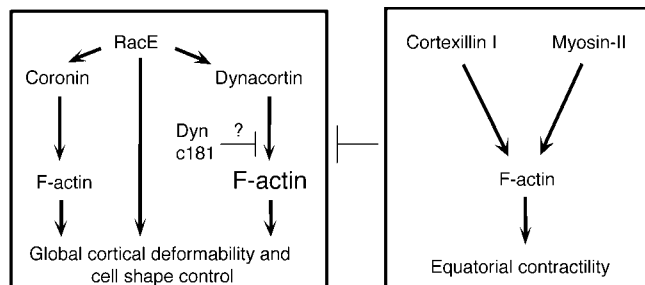


FIG. 7. A working model to integrate the genetics, cell biology, and biochemistry of cytokinesis in *Dictyostelium discoideum* (3). In this model, two modules are proposed to interact to promote cell division. A global pathway is presided over by RacE and includes coronin and dynacortin. This pathway may control the global shape and material properties (stiffness) of the cell. The global pathway is antagonized by the equatorial pathway, which includes cortexillin I and myosin-II. Myosin-II generates contractile force and cortexillin I cross-links actin filaments, possibly to generate a localized increase in stiffness. Dynacortin was isolated because a construct that encodes only the carboxyl-terminal 181 amino acids rescued mutants devoid of cortexillin I. This construct may act as a dominant-negative protein that inhibits normal dynacortin function. In this paper, we demonstrate that dynacortin also acts on the actin-filament network, cross-linking it into arrays. Together, these data point toward interacting modules that act upon the actin filament cytoskeleton to orchestrate the complex cell shape changes of cytokinesis.

tion to the lateral cortex (3). Perhaps RacE recruits and regulates dynacortin-mediated actin filament cross-linking by regulating a kinase for dynacortin. Rac-family proteins also activate IQGAP proteins, which modulate and regulate the recruitment of the actin-myosin cytoskeleton to the bud neck in yeast (23, 24). Two IQGAP proteins have been invoked in modulating Rac1-mediated cytoskeletal changes in *D. discoideum* (25). These proteins have been shown to form a complex with the cortexillins and to be required for normal recruitment of the cortexillins to the cleavage furrow cortex (26). These same IQGAP proteins or other related proteins could modulate dynacortin's localization and activity. Other Rac family proteins may also regulate dynacortin recruitment and/or actin cross-linking in other cortical structures such as actin crowns and phagocytic cups (27, 28).

Finally, since dynacortin is a novel protein with such an unusual amino acid composition, discerning its actin bundling mechanism will be of interest. It is particularly intriguing that a single protein can drive the formation of such distinct actin bundle structures, actin bundle networks, and actin bundle rings. Dynacortin's ability to bundle filaments into rings is intriguing since the protein is found *in vivo* to localize to circular rings of actin such as actin crowns and phagocytic cups (3). While other actin bundling proteins may be able to form such structures, here we demonstrate that only actin filaments and dynacortin are necessary to form rings *in vitro*. Dynacortin might be able to bear some load since an actin filament has a persistence length of $9 \mu\text{M}$ (29) and many of the rings are as small as $2 \mu\text{M}$ in diameter ($6 \mu\text{M}$ circumference; $1 \mu\text{M}$ radius of curvature). Since dynacortin-actin rings can be easily assem-

bled *in vitro*, in future work we will be able to study their assembly pathways and structure. This may serve as a useful model for other types of actin ring structures that are found elsewhere in nature such as in the intercellular bridges that connect germline cells in a variety of metazoans (reviewed in Ref. 30).

Although a direct connection to the Arp2/3 complex seems unlikely, a question still remains as to why dynacortin co-fractionates with the Arp2/3 complex so extensively. The most likely explanation is that since both have a common interactor, actin filaments, the co-fractionation may reflect a similar charge distribution on each of the protein complexes. It is certain that the Stokes radius similarity is serendipitous. However, it is intriguing that the Arp2/3 complex localizes to cell surface protrusions and is found most concentrated at the poles of the cell during cytokinesis (31), which are similar to the patterns of localization seen for dynacortin (3). So far, preliminary experiments have not indicated an effect by dynacortin on Arp2/3-mediated nucleation of actin polymerization. However, we are exploring the types of structures that might be built from Arp2/3-nucleated dendritic actin meshworks (32) that are then bundled by dynacortin.

Acknowledgments—We thank John Dawson and Matt Footer for advice on protein purification, Dan Hostetter and Pehr Harbury for advice on analytical ultracentrifugation, Dick Winant from the Stanford PAN facility for help with mass spectrometry, and Nafisa Ghorri from the Stanford Immunology Electron Microscopy facility for assistance with electron microscopy. We thank the members of the Spudich lab for helpful comments on the manuscript.

REFERENCES

- Robinson, D. N. (2001) *Curr. Biol.* **11**, R737–R740
- Robinson, D. N., and Spudich, J. A. (2000) *Trends Cell Biol.* **10**, 228–237
- Robinson, D. N., and Spudich, J. A. (2000) *J. Cell Biol.* **150**, 823–838
- DeLozanne, A., and Spudich, J. A. (1987) *Science* **236**, 1086–1091
- Faix, J., Steinmetz, M., Boves, H., Kammerer, R. A., Lottspeich, F., Mintert, U., Murphy, J., Stock, A., Aebi, U., and Gerisch, G. (1996) *Cell* **86**, 631–642
- Weber, I., Neujahr, R., Du, A., Köhler, J., Faix, J., and Gerisch, G. (2000) *Curr. Biol.* **10**, 501–506
- deHostas, E. L., Rehfuß, C., Bradtke, B., Waddell, D. R., Albrecht, R., Murphy, J., and Gerisch, G. (1993) *J. Cell Biol.* **120**, 163–173
- Larochelle, D. A., Vithalani, K. K., and DeLozanne, A. (1996) *J. Cell Biol.* **133**, 1321–1329
- Gerald, N., Dai, J., Ting-Beall, H. P., and DeLozanne, A. (1998) *J. Cell Biol.* **141**, 483–492
- Pasternak, C., Spudich, J. A., and Elson, E. L. (1989) *Nature* **341**, 549–551
- Simson, R., Wallraff, E., Faix, J., Niewöhner, J., Gerisch, G., and Sackmann, E. (1998) *Biophys. J.* **74**, 514–522
- Moore, S. L., Sabry, J. H., and Spudich, J. A. (1996) *Proc. Natl. Acad. Sci. U. S. A.* **93**, 443–446
- Weber, I., Gerisch, G., Heizer, C., Murphy, J., Badelt, K., Stock, A., Schwartz, J.-M., and Faix, J. (1999) *EMBO J.* **18**, 586–594
- Manstein, D. J., Schuster, H.-P., Morandini, P., and Hunt, D. M. (1995) *Gene (Amst.)* **162**, 129–134
- Laue, T. M., Shah, B. D., Ridgeway, T. M., and Pelletier, S. L. (1992) in *Analytical Ultracentrifugation in Biochemistry and Polymer Science* (Harding, S., Rowe, A., and Horton, J. C., eds) Royal Society of Chemistry, Cambridge, United Kingdom
- Pardee, J. D., and Spudich, J. A. (1982) *Methods Cell Biol.* **24**, 271–289
- Mullins, R. D., and Machesky, L. M. (2000) *Methods Enzymol.* **325**, 214–237
- Loomis, W. (1987) *Methods Cell Biol.* **28**, 31–65
- Higgs, H. N., and Pollard, T. D. (1999) *J. Biol. Chem.* **274**, 32531–32534
- Welch, M. D. (1999) *Trends Cell Biol.* **9**, 423–427
- Matzke, R., Jacobson, K., and Radmacher, M. (2001) *Nat. Cell Biol.* **3**, 607–610
- Haugwitz, M., Noegel, A. A., Karakesisoglou, J., and Schleicher, M. (1994) *Cell* **79**, 303–314
- Boyne, J. R., Yusuf, H. M., Bieganowski, P., Brenner, C., and Price, C. (2000) *J. Cell Sci.* **113**, 4533–4543
- Shannon, K. B., and Li, R. (1999) *Mol. Biol. Cell* **10**, 283–296
- Faix, J., Clougherty, C., Konzok, A., Mintert, U., Murphy, J., Albrecht, R., Mühlbauer, B., and Kuhlmann, J. (1998) *J. Cell Sci.* **111**, 3059–3071
- Faix, J., Weber, I., Mintert, U., Köhler, J., Lottspeich, F., and Marriotti, G. (2001) *EMBO J.* **20**, 3705–3715
- Rivero, F., Albrecht, R., Dislich, H., Bracco, E., Graciotti, L., Bozzaro, S., and Noegel, A. A. (1999) *Mol. Biol. Cell* **10**, 1205–1219
- Seastone, D. J., Lee, E., Bush, J., Knecht, D., and Cardelli, J. (1998) *Mol. Biol. Cell* **9**, 2891–2904
- Howard, J. (2001) *Mechanics of Motor Proteins and the Cytoskeleton*, Sinauer Associates, Sunderland, MA
- Robinson, D. N., and Cooley, L. (1996) *Trends Cell Biol.* **6**, 474–479
- Insall, R., Mueller-Tautenberg, A., Machesky, L., Koehler, J., Simmeth, E., Atkinson, S. J., Weber, I., and Gerisch, G. (2001) *Cell Motil. Cytoskeleton* **50**, 115–128
- Svitkina, T. M., and Borisy, G. G. (1999) *J. Cell Biol.* **145**, 1009–1026